

A MODIFIED FLOWFIELD DEPENDENT VARIATION METHOD APPLIED TO THE COMPRESSIBLE EULER FLOW EQUATIONS

A. A. Megahed[†], M. W. El-Mallah[§], B. R. Girgis[‡]

Engineering Mathematics and Physics Department,
Faculty of Engineering,
Cairo University, Giza, Egypt, 12613

ABSTRACT

In the present work the flowfield dependent variation method (FDV), originally developed by T. J. Chung and his co-workers, has been modified to improve the physical meaning of the used variation (implicitness) parameters. The modified method (MFDV) has been applied to the compressible Euler flow equations. While finite difference techniques are applicable for solving the resulting system of equations, finite element discretization has been used via standard Galerkin method. This choice has been made for two reasons, to take the well-known advantages of the finite element techniques, and to maximize the benefits from the gained physical meaning by the MFDV method. A number of famous test cases have been solved to prove the applicability of the proposed modification and a good agreement with the published literature has been obtained.

KEYWORDS

Computational Fluid Dynamics (CFD), Flowfield Dependent Variation (FDV) method, Euler equations, Finite Element (FE), Galerkin method, Modified Flowfield Dependent Variation (MFDV) method

NOMENCLATURE

\mathbf{a}_i	$= \partial \mathbf{F}_i / \partial \mathbf{U}$ convection Jacobian tensor
c_v, R	specific heat at constant volume and gas constant
e, e_t	static and total internal energy
\mathbf{F}	convection flux

i, j	co-ordinate dimension counters = 1,2
L^*	element characteristic length
M	Mach No.
n_i	boundary normal vector
P, T	pressure and temperature
s_1, s_2	1 st and 2 nd order convection FDV implicitness parameters
$t, \Delta t$	time and time step
u_i	velocity components in 2-D space
\mathbf{U}	conservation variables vector
x_i	space co-ordinates
α, β	nodal element counters = 1,2,3,4 for quadrilateral elements
Φ, Φ^*	domain and boundary shape functions
γ	specific heat ratio
ρ	density
Ω, Γ	domain and contour boundaries
$\nabla ()$	gradient of a scalar function

INTRODUCTION

Many practical CFD problems in industry and research attain crucial flow situations. To accurately predict flow properties, the solution technique should be able to handle the strong interactions between high and low speeds, subsonic-transonic-supersonic, viscous and inviscid flows for both compressible and incompressible cases. In the recent decades, all the CFD research efforts ([2]-[8]) were directed towards the development of numerical techniques that are able to operate

[†] Professor, adelam@menanet.net

[§] Assistant Professor, mouradmallah@yahoo.com

[‡] Research/Teaching Assistant, brguirguis@yahoo.com

on different flow regimes seamlessly. FDV method has been devised as a response to this demand ([3] and [9]).

EULER EQUATIONS IN 2-D SPACE

The system of compressible Euler flow equations can be written in the conservation form as follows:

$$\frac{\partial \mathbf{U}}{\partial t} + \frac{\partial \mathbf{F}_i}{\partial x_i} = 0 \quad (1)$$

Where; in 2-D space the conservation variables vector is given by:

$$\mathbf{U} = [\rho \quad \rho u_1 \quad \rho u_2 \quad \rho e_t]^T \quad (2)$$

Also the convection flux is given by:

$$\mathbf{F} = \begin{bmatrix} \rho u_1 & \rho u_2 \\ \rho u_1^2 + P & \rho u_1 u_2 \\ \rho u_1 u_2 & \rho u_2^2 + P \\ \rho u_1 e_t + P u_1 & \rho u_2 e_t + P u_2 \end{bmatrix} \quad (3)$$

$$P = \rho R T \quad (4)$$

$$e = c_v T \quad (5)$$

Eqn. (1) with the ideal gas equation of state, Eqn. (4), and the thermally perfect gas assumption, Eqn. (5), completes the system of Euler's flow equations.

Rewriting Eqn. (1) in a quasi-linear form as follows:

$$\frac{\partial \mathbf{U}}{\partial t} + \mathbf{a}_i \frac{\partial \mathbf{U}}{\partial x_i} = 0 \quad (6)$$

Where; \mathbf{a}_i is the convection Jacobian tensor¹ which is considered to be time-step dependent.

FDV METHOD FORMULATION

For a detailed step by step derivation of the FDV method, the reader is referred to [1], [2], and [9]. The FDV method can be summarized in the following steps:

a) Expanding \mathbf{U}^{n+1} around \mathbf{U}^n in a special form of Taylor expansion.

$$\mathbf{U}^{n+1} = \mathbf{U}^n + \Delta t \frac{\partial \mathbf{U}^{n+s_1}}{\partial t} + \frac{(\Delta t)^2}{2} \frac{\partial^2 \mathbf{U}^{n+s_2}}{\partial t^2} + O((\Delta t)^3)$$

Where;

$$\frac{\partial \mathbf{U}^{n+s_1}}{\partial t} = \frac{\partial \mathbf{U}^n}{\partial t} + s_1 \frac{\partial \Delta \mathbf{U}^{n+1}}{\partial t} \quad 0 \leq s_1 \leq 1$$

$$\frac{\partial^2 \mathbf{U}^{n+s_2}}{\partial t^2} = \frac{\partial^2 \mathbf{U}^n}{\partial t^2} + s_2 \frac{\partial^2 \Delta \mathbf{U}^{n+1}}{\partial t^2} \quad 0 \leq s_2 \leq 1$$

$$\Delta \mathbf{U}^{n+1} = \mathbf{U}^{n+1} - \mathbf{U}^n$$

The implicitness parameters, s_1 and s_2 , are flowfield dependent. They may gain their physical meaning by being calculated from the flow variables' fluctuations. The proposed formula by T. J. Chung in [9] for calculating s_1, s_2 from the current flowfield is given by:

$$s_1 = \begin{cases} \min(r, 1) & r > \varepsilon \\ 0 & r < \varepsilon, M_{\min} \neq 0 \\ 1 & M_{\min} = 0 \end{cases} \quad (7)$$

$$s_2 = \frac{1}{2}(1 + s_1^\eta), \quad 0.05 < \eta < 0.2 \quad (8)$$

Where;

$r = \sqrt{M_{\max}^2 - M_{\min}^2} / M_{\min}$, ε is a small number, and M_{\min}, M_{\max} are the minimum and maximum values of the Mach No. in the neighboring nodes (i.e. between the element nodes).

b) Substituting from Eqn. (6) into the Taylor expansion by interchanging the time derivatives with the spatial derivatives we get:

$$\begin{aligned} \Delta \mathbf{U}^{n+1} = & \Delta t \left(-\frac{\partial \mathbf{F}_i^n}{\partial x_i} - s_1 \frac{\partial \Delta \mathbf{F}_i^{n+1}}{\partial x_i} \right) + \\ & + \frac{(\Delta t)^2}{2} \mathbf{a}_i \frac{\partial}{\partial x_i} \left(\frac{\partial \mathbf{F}_j^n}{\partial x_j} \right) + \\ & + \frac{(\Delta t)^2}{2} s_2 \mathbf{a}_i \frac{\partial}{\partial x_i} \left(\frac{\partial \Delta \mathbf{F}_j^{n+1}}{\partial x_j} \right) + \\ & + O((\Delta t)^3) \end{aligned} \quad (9)$$

c) Rewriting Eqn. (9) in the residual form and substituting all the Δ terms with their Jacobian equivalents we get:

$$\begin{aligned} \Delta \mathbf{U}^{n+1} + \Delta t s_1 \mathbf{a}_i \frac{\partial}{\partial x_i} (\Delta \mathbf{U}^{n+1}) + \\ - \frac{(\Delta t)^2}{2} s_2 \mathbf{a}_i \mathbf{a}_j \frac{\partial^2}{\partial x_i \partial x_j} (\Delta \mathbf{U}^{n+1}) + \\ + \Delta t \frac{\partial \mathbf{F}_i^n}{\partial x_i} - \frac{(\Delta t)^2}{2} \mathbf{a}_i \frac{\partial}{\partial x_i} \left(\frac{\partial \mathbf{F}_j^n}{\partial x_j} \right) + \\ + O((\Delta t)^3) = 0 \end{aligned} \quad (10)$$

Rearranging Eqn. (10):

¹ See the appendix.

$$\begin{aligned} &\Delta \mathbf{U}^{n+1} + \mathbf{D}_i^n \frac{\partial}{\partial x_i} (\Delta \mathbf{U}^{n+1}) + \\ &+ \mathbf{E}_{ij}^n \frac{\partial^2}{\partial x_i \partial x_j} (\Delta \mathbf{U}^{n+1}) + \mathbf{Q}^n + \\ &+ \mathcal{O}((\Delta t)^3) = 0 \end{aligned} \quad (11)$$

Where;

$$\begin{aligned} \mathbf{D}_i^n &= \Delta t s_1 \mathbf{a}_i, \quad \mathbf{E}_{ij}^n = -\frac{(\Delta t)^2}{2} s_2 \mathbf{a}_i \mathbf{a}_j, \quad \text{and} \\ \mathbf{Q}^n &= \Delta t \frac{\partial}{\partial x_i} (\mathbf{F}_i^n) - \frac{(\Delta t)^2}{2} \mathbf{a}_i \frac{\partial^2}{\partial x_i \partial x_j} (\mathbf{F}_j^n) \end{aligned}$$

Eqn. (11) can be solved either by finite difference methods or finite element methods. The latter has been chosen for two reasons: to take the well-known advantages of the finite element techniques, and to maximize the benefits from the gained physical meaning by the MFDV method.

FINITE ELEMENT DISCRETIZATION: STANDARD GALERKIN METHOD

From the standard Galerkin method we have:

$$\int_{\Omega} \Phi_{\alpha} \mathbf{R}(\mathbf{U}, \mathbf{F}) d\Omega = 0 \quad (12)$$

Where; $\mathbf{R}(\mathbf{U}, \mathbf{F})$ is the residual of Eqn. (11)

In what follows the order of the solution error $\mathcal{O}((\Delta t)^3)$ will be omitted for convenience.

Expressing the conservation variables vector as a linear combination of the trial functions Φ_{α} we have:

$$\mathbf{U}(\mathbf{x}, t) = \Phi_{\alpha}(\mathbf{x}) \mathbf{U}_{\alpha}(t) \quad (13)$$

Performing integration by parts:

$$\begin{aligned} &\int_{\Omega} \Phi_{\alpha} \Phi_{\beta} \Delta \mathbf{U}_{\beta}^{n+1} d\Omega + \\ &+ \int_{\Gamma} \mathbf{D}_i^n \Phi_{\alpha} \Phi_{\beta} \Delta \mathbf{U}_{\beta}^{n+1} n_i d\Gamma + \\ &- \int_{\Omega} \mathbf{D}_i^n \Phi_{\alpha,i} \Phi_{\beta} \Delta \mathbf{U}_{\beta}^{n+1} d\Omega + \\ &+ \int_{\Gamma} \mathbf{E}_{ij}^n \Phi_{\alpha} \Phi_{\beta,j} \Delta \mathbf{U}_{\beta}^{n+1} n_i d\Gamma + \\ &- \int_{\Omega} \mathbf{E}_{ij}^n \Phi_{\alpha,i} \Phi_{\beta,j} \Delta \mathbf{U}_{\beta}^{n+1} d\Omega + \\ &+ \Delta t \int_{\Gamma} \Phi_{\alpha} \mathbf{F}_i^n n_i d\Gamma - \Delta t \int_{\Omega} \Phi_{\alpha,i} \mathbf{F}_i^n d\Omega + \\ &- \frac{(\Delta t)^2}{2} \int_{\Gamma} \mathbf{a}_i \Phi_{\alpha} \frac{\partial}{\partial x_j} (\mathbf{F}_j^n) n_i d\Gamma + \end{aligned}$$

$$+ \frac{(\Delta t)^2}{2} \int_{\Omega} \mathbf{a}_i \Phi_{\alpha,i} \frac{\partial}{\partial x_j} (\mathbf{F}_j^n) d\Omega = 0$$

Rearranging these terms:

$$\boxed{(\mathbf{A}_{\alpha\beta}^n + \mathbf{B}_{\alpha\beta}^n) \Delta \mathbf{U}_{\beta}^{n+1} = \mathbf{H}_{\alpha}^n + \mathbf{N}_{\alpha}^n} \quad (14)$$

Where;

$$\mathbf{A}_{\alpha\beta}^n = \int_{\Omega} (\Phi_{\alpha} \Phi_{\beta} - \mathbf{D}_i^n \Phi_{\alpha,i} \Phi_{\beta} - \mathbf{E}_{ij}^n \Phi_{\alpha,i} \Phi_{\beta,j}) d\Omega$$

$$\mathbf{B}_{\alpha\beta}^n = \int_{\Gamma} (\mathbf{D}_i^n \Phi_{\alpha} \Phi_{\beta} + \mathbf{E}_{ij}^n \Phi_{\alpha} \Phi_{\beta,j}) n_i d\Gamma$$

$$\mathbf{H}_{\alpha}^n = \int_{\Omega} \left(\Delta t \Phi_{\alpha,i} \mathbf{F}_i^n - \frac{(\Delta t)^2}{2} \mathbf{a}_i \Phi_{\alpha,i} \frac{\partial}{\partial x_j} (\mathbf{F}_j^n) \right) d\Omega$$

$$\mathbf{N}_{\alpha}^n = \int_{\Gamma} \left(-\Delta t \Phi_{\alpha} \mathbf{F}_i^n + \frac{(\Delta t)^2}{2} \mathbf{a}_i \Phi_{\alpha} \frac{\partial}{\partial x_j} (\mathbf{F}_j^n) \right) n_i d\Gamma$$

Eqn (14) is referred to as the element equations.

It is important to remember that by setting $s_1 = 0$ and $s_2 = 1$, the so called Taylor-Galerkin method is obtained. Actually, any known numerical scheme in either finite element or finite difference may rise as a special case of the FDV method with s_1 and s_2 fixed to certain values. For a comprehensive comparison between FDV and other methods the reader is referred to [6]. Allowing the implicitness parameters (s_1, s_2) to vary from element to element gives the FDV method the ability to provide a unique and distinctive numerical scheme for each element according to its current flowfield values.

MODIFIED THEORY: THE MFDV METHOD

In the proposed method (MFDV), the relation used to recover the first order implicitness parameter (Eqn. (7)) from the current flowfield data is modified to give this parameter a deeper physical meaning. This can be accomplished by setting s_1 to be proportional to the first order derivative of the Mach No. This is quite equivalent to the definition of s_1 given in [2]-[4], [6]. Also to retain the dimensional similarity the result is multiplied by the elemental characteristic length and scaled by the minimal Mach No. between the element nodes. The proposed modification is given by:

$$s_1 = \min(r, 1) \quad (15)$$

Where;

$$r = L^* |\nabla M| / M_{\min}$$

And the other implicitness parameter (s_2) is calculated as in Eqn. (8).

The authors would like to admit the applicability and effectiveness of the original formula proposed by T. J. Chung and his co-workers. The current work is a step towards deeper understanding of the role of the implicitness parameters.

BOUNDARY CONDITIONS

It is well known that an efficient and robust boundary conditions implementation technique is a crucial issue for all CFD problems. In this section the most important boundary conditions are discussed. These boundary conditions are used to simulate many practical flow situations encountered in real flow problems.

a) Inviscid Wall Boundary Condition (No Penetration)

There is many ways to implement the wall boundary conditions inside the Euler solver. One of the most successful methods is the method of co-ordinates rotation given in Reddy [10] and implemented successfully by many others including F. Moussaoui [7], T. E. Tezduyar et al. [8]. In this method the velocity components at the solid wall are transformed to the normal and tangential components, as shown in Figure 1.

These axes are used to introduce the zero normal velocity ($u_n = 0.0$) via equating the normal component to zero. The coordinate transformation matrix will take the form:

$$\begin{pmatrix} u_1 \\ u_2 \end{pmatrix} = \begin{pmatrix} \cos \theta & -\sin \theta \\ \sin \theta & \cos \theta \end{pmatrix} \begin{pmatrix} u_t \\ u_n \end{pmatrix}$$

For the nodes on the solid boundary a new vector of unknowns is to be introduced via the following rotation matrix:

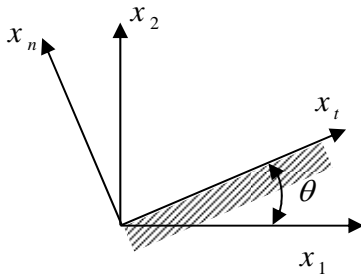


Figure 1 Co-ordinates rotation at a solid wall

$$\begin{pmatrix} \rho \\ \rho u_t \\ \rho u_n \\ \rho e_t \end{pmatrix} = \begin{pmatrix} 1 & 0 & 0 & 0 \\ 0 & \cos \theta & \sin \theta & 0 \\ 0 & -\sin \theta & \cos \theta & 0 \\ 0 & 0 & 0 & 1 \end{pmatrix} \begin{pmatrix} \rho \\ \rho u_1 \\ \rho u_2 \\ \rho e_1 \end{pmatrix}$$

b) Supersonic Inlet Boundary Condition

For all the nodes on the supersonic inlet boundary, the four flow properties ($\rho, \rho u_1, \rho u_2, \rho e_1$) should be specified exactly.

c) Supersonic Exit Boundary Condition Left free

NUMERICAL RESULTS

Many problems have been solved to validate the applicability and effectiveness of the MFDV method. All the test cases have been solved using Fortran 90 code and a preconditioned GMRES sparse matrix solver (see [11] and [12]). In this section we present only two test cases.

Shock Reflection Problem

The solution domain of shock reflection from inviscid wall, as shown in Figure 2, is discretized uniformly with 60x20 bilinear rectangular elements.

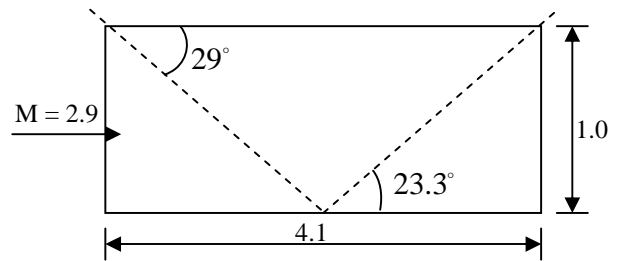


Figure 2 Shock reflection

At both inlet and upper boundaries, the supersonic inlet boundary condition is used with the following values:

Inlet:

$$\begin{aligned} \rho &= 1.0, & \rho u_1 &= 2.9, \\ \rho u_2 &= 0.0, & \rho e_1 &= 5.99075 \end{aligned}$$

Upper:

$$\begin{aligned} \rho &= 1.7, & \rho u_1 &= 4.453, \\ \rho u_2 &= -0.86, & \rho e_1 &= 9.87 \end{aligned}$$

On lower boundary, the inviscid wall (no-penetration) boundary condition is used and the exit boundary is left free being supersonic exit.

Figure 4 shows the Mach No. contours. Our results matches very well the results obtained in [13]. Figure 5 shows the contours of s_1 while Figure 6 shows the contours of s_2 . It is clear that s_1 parameter resolves the solution itself and this interesting property for s_1 may be utilized if an adaptation technique is to be used.

Figure 7 shows a comparison between the Mach No. at $y = 0.5$ from this test case and a more refined grid (120x60) with the exact analytical solution. It is clear that as the grid gets finer the exact solution is approached. Also a higher over/undershoots can be observed for finer grids. This is due to the lost solution modes resulting from the grid selectivity.

Compression Corner Problem

The compression corner problem is shown in Figure 3. The solution domain is discretized using 60x40 bilinear quadrilateral elements with expansion ratio of 1.02 in the lateral direction.

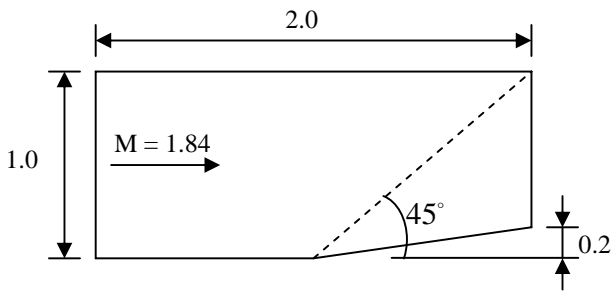


Figure 3 Compression corner

The inlet boundary is supersonic and the following values have been used:

$$\begin{aligned} \rho &= 1.0, & \rho u_1 &= 1.84, \\ \rho u_2 &= 0.0, & \rho e_t &= 3.47855 \end{aligned}$$

The no-penetration boundary condition is applied on both the upper and lower boundaries and the exit boundary is left free being supersonic.

Figure 9 shows the Mach No. contours. The shown results matches very well the results of the analytical solution given from the oblique shock wave theory. Figure 10 shows the contours of s_1 and Figure 11 shows the contours of s_2 .

Figure 8 is a comparison between the Mach No. at $y = 0.5$ from this test case and a relatively fine grid (120x80) with the exact analytical solution. The same trend that was observed at the first test case has, also, attained in this test case.

CONCLUSIONS

MFDV method is capable of recovering the implicitness parameters and it gave a satisfactory performance in the tested problems. This work is considered to be an attempt towards

deeper understand of the implicitness parameters and more accurate calculations of s_1 and s_2 . The authors expect to publish an extension of this work to the solution of the Navier-Stokes equations very soon. Also they expect to publish more results to demonstrate the capabilities of both FDV and MFDV.

ACKNOWLEDGMENTS

The authors would like to acknowledge Prof. T. J. Chung for his discussions regarding the original FDV method.

APPENDIX

The 2-D convection Jacobian, \mathbf{a}_i , is given by:

\mathbf{a}_1

0	1	0	0
a_{21}^1	$(3-\gamma)u_1$	$(1-\gamma)u_2$	$(\gamma-1)$
$-u_1 u_2$	u_2	u_1	0
a_{41}^1	a_{42}^1	$(1-\gamma)u_1 u_2$	γu_1

$$a_{21}^1 = \frac{1}{2}((\gamma-3)u_1^2 + (\gamma-1)u_2^2)$$

$$a_{41}^1 = -u_1((1-\gamma)(u_1^2 + u_2^2) + \gamma e_t)$$

$$a_{42}^1 = \gamma e_t + \frac{(1-\gamma)}{2}(3u_1^2 + u_2^2)$$

\mathbf{a}_2

0	0	1	0
$-u_1 u_2$	u_2	u_1	0
a_{31}^2	$(1-\gamma)u_1$	$(3-\gamma)u_2$	$(\gamma-1)$
a_{41}^2	$(1-\gamma)u_1 u_2$	a_{43}^2	γu_2

$$a_{31}^2 = \frac{1}{2}((\gamma-3)u_2^2 + (\gamma-1)u_1^2)$$

$$a_{41}^2 = -u_2((1-\gamma)(u_1^2 + u_2^2) + \gamma e_t)$$

$$a_{43}^2 = \gamma e_t + \frac{(1-\gamma)}{2}(u_1^2 + 3u_2^2)$$

REFERENCES

- [1] B. R. Girgis, *Flowfield-Dependent Variation Method Applied to Compressible Euler and Navier-Stokes Equations*, Master Thesis, Eng. Mathematics and Physics Dept., Cairo University, Giza, Egypt, 2006.

- [2] Chung, T. J., *Transitions and interactions of inviscid/viscous, compressible/incompressible and laminar/turbulent flows*, Int. J. for Num. Meth. in fl., 31.223-46 (1999).
- [3] Schunk, R.G., Gunabal, Heard, G. W., and Chung, T. J., *Unified CFD methods via flowfield-dependent variation theory*, AIAA 99 (1999)-3715.
- [4] Yoon, K. T. and Chung, T. J., *Three dimensional mixed explicit-implicit generalized Galerkin spectral elements methods for high speed turbulent compressible flows*, Comp. Methods. Appl. Mech. Engrg. 135 (1996), 343-67.
- [5] F. Shakib, Thomas J. R. Hughes. Zdenek Johan, *A new finite element formulation for computational fluid dynamics: X. The compressible Euler and Navier-Stokes equations*, Comp. Methods. Appl. Mech. Engrg. 89 (1991), 141-219.
- [6] K. T. Yoon, S. Y. Moon, S. A. Garcia, G. W. Heard, T. J. Chung, *Flowfield-dependent mixed explicit (FDMEI) methods for high and low speed and compressible and incompressible flows*, Comput. Methods. Appl. Mech. Engrg. 151 (1998), 75-104.
- [7] F. Moussaoui, *A unified approach for inviscid compressible and nearly incompressible flow by least-squares finite element method*, Appl. Num. Math. 44 (2003), 183-199.
- [8] G. J. Le Beau, T. E. Tezduyar, *Finite element computations of compressible flows with the SUPG formulation*, ASME, FED. Vol. 123 (1991), Advances in finite element analysis in fluid dynamics.
- [9] T. J. Chung, *Computational Fluid Dynamics*, Cambridge press (2002).
- [10] J. N. Reddy, *An Introduction to the Finite Element Method*, 2nd edition. McGraw-Hill Book Co. (1993).
- [11] Youcef Saad and Martin H. Schultz, *GMRES: A new generalized minimal residual algorithm for solving nonsymmetric linear systems*, Society for industrial and app. Math., Vol 7, No 3 (1986), pp. 856-869.
- [12] Youcef Saad, *A flexible inner-outer preconditioning GMRES algorithm*, Society for industrial and app. Math., Vol 14, No 2 (1993), pp. 461-469.
- [13] F. Taghaddosi, W. G. Habashi, G. Guevremont, and D. Ait-Ali-Yahia, *An adaptive least square method for the compressible Euler equations*, AIAA-97-2097.

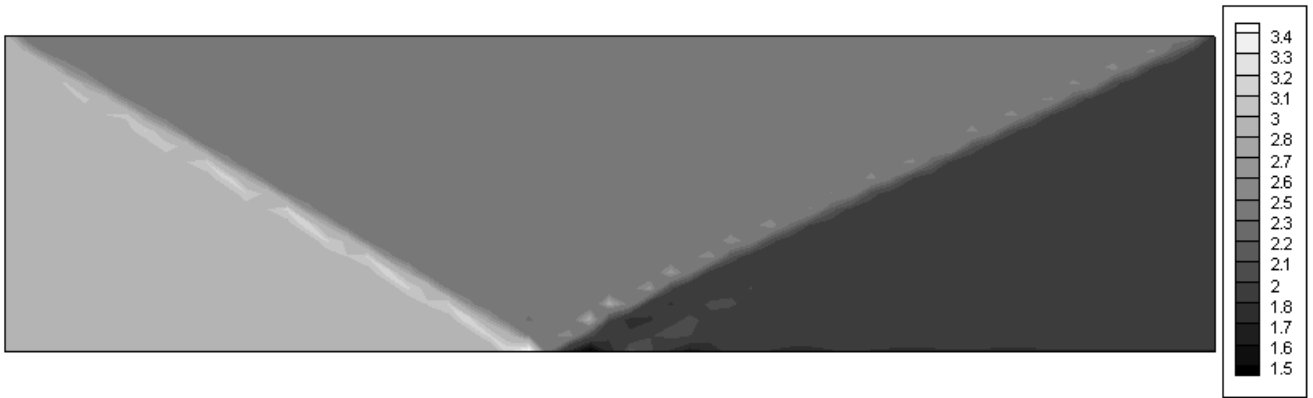


Figure 4 Mach No. contours for shock-reflection test case, 60x20

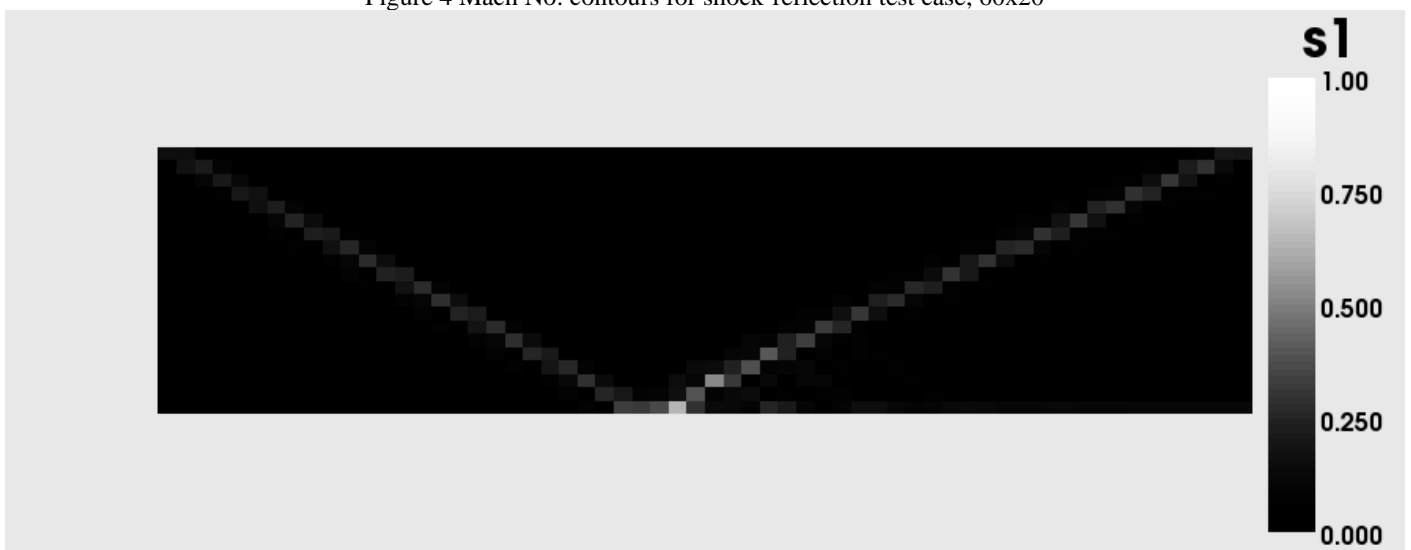


Figure 5 The first order implicitness parameter s_1 contours for shock-reflection test case, 60x20



Figure 6 The second order implicitness parameter s_2 contours for shock-reflection test case, 60x20

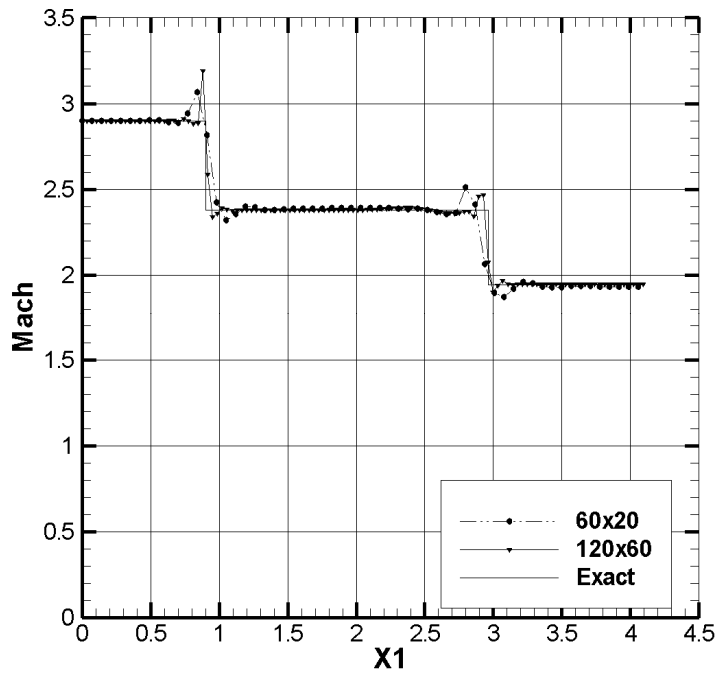


Figure 7 Comparison between different grids and the analytical solution for shock-reflection test case at $y = 0.5$

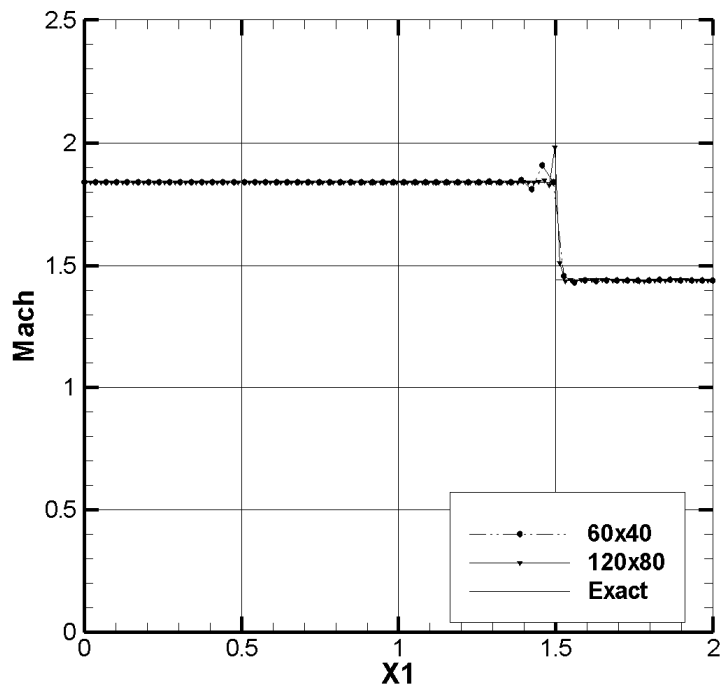


Figure 8 Comparison between different grids and the analytical solution for compression-corner test case at $y = 0.5$



Figure 9 Mach No. contours for compression-corner test case, 60x40

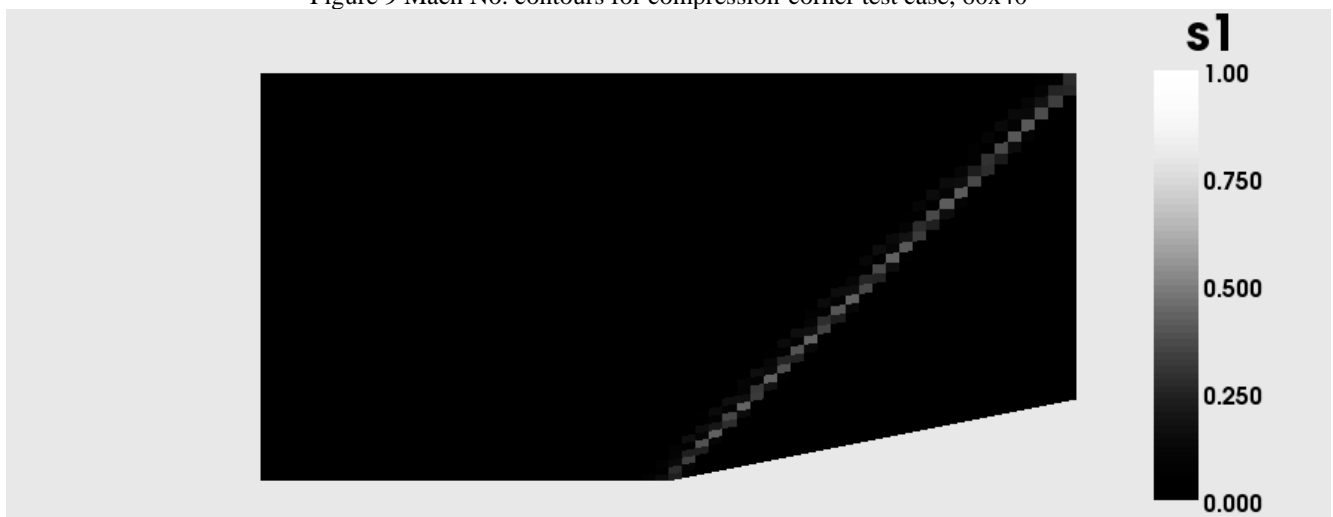


Figure 10 The first order implicitness parameter s_1 contours for compression-corner test case, 60x40

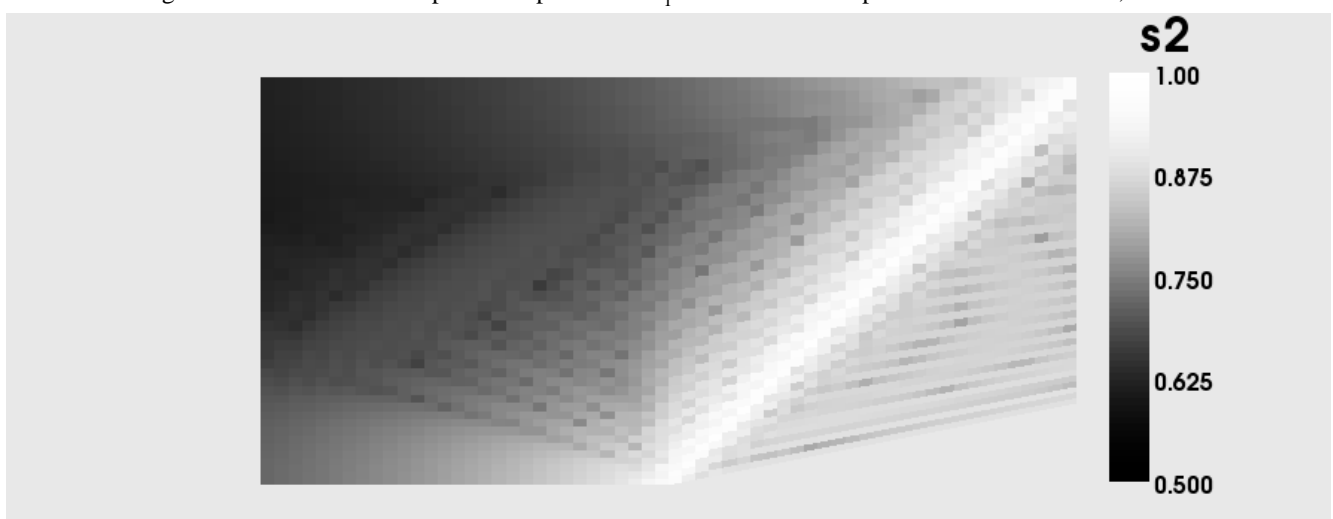


Figure 11 The second order implicitness parameter s_2 contours for compression-corner test case, 60x40